

Modeling the Spatial Distribution of Neutron Stars in the Galaxy

Ali Taani, Luca Naso, Yingchun Wei, Chengmin Zhang and Yongheng Zhao
National Astronomical Observatories, Chinese Academy of Sciences, Beijing 100012, China
 alitaani@bao.ac.cn

ABSTRACT

In this paper we investigate the space and velocity distributions of old neutron stars (aged 10^9 to 10^{10} yr) in our Galaxy. Galactic old Neutron Stars (NSs) population fills a torus-like area extending to a few tens kiloparsecs above the galactic plane. The initial velocity distribution of NSs is not well known, in this work we adopt a three component initial distribution, as given by the contribution of kick velocities, circular velocities and Maxwellian velocities. For the spatial initial distribution we use a Γ function. We then use Monte Carlo simulations to follow the evolution of the NSs under the influence of the Paczyński Galactic gravitational potential. Our calculations show that NS orbits have a very large Galactic radial expansion and that their radial distribution peak is quite close to their progenitors' one. We also study the NS vertical distribution and find that it can well be described by a double exponential low. Finally, we investigate the correlation of the vertical and radial distribution and study the radial dependence of scale-heights.

Subject headings: Pulsar: general — galaxies: The Galaxy — Galaxy: disk — galaxies: kinematics and dynamics — stars: statistics

1. Introduction

It is commonly accepted that Neutron Stars (NSs) are born when massive OB-stars exhaust their nuclear fuel and end their lives in core-collapse supernova explosions, near the Galactic disk (see e.g. Bhattacharya & van den Heuvel (1991)) and that they have then moved away from the Galactic plane with average kick velocities around 200 – 500 km/s (e.g. Cordes & Chernoff (1998), Lyne et al. (2004), Hobbs et al. (2005)). About 10^9 NSs are thought to populate our Galaxy, but only 2×10^3 are directly observed as radio pulsars or as accretion-powered Xray binaries (Sartore et al. 2010), as a consequence, little is known about their statistical properties. The estimation of pulsar velocities relies on direct distance measurements, which can be obtained by dispersion measures together with a Galactic electron density model (e.g. Taylor & Cordes (1993), Cordes & Lazio (2002)). The mechanisms for producing high velocities are still unknown (Lorimer 2008).

Numerical simulations are valuable tools for understanding the spatial and velocity distribution of NSs in the Galaxy, and they have been used by several authors (see e.g. Caldwell & Ostriker (1981), Ofek (2009), Katsanikas & Patsis (2011)). In particular, Paczyński (1990) (hereafter P90) simulated the motion of NSs in connection with the galactic origin of gamma ray bursts and calculated the NS space density distribution. In the same work Paczyński also suggested a simplified expression for the gravitational potential which is still often applied in the simulation of NS distribution. For example Wei et al. (2010a) used this potential. They considered the old NSs, i.e. NSs whose age is between 10^9 and 10^{10} yr. They adopted a Galactic distribution with one-component initial random velocity models. The aim of the present work is to improve the model developed in Wei et al. (2010a) for studying the distribution of old NSs as a function of the initial position distribution, of the initial velocity distribution and of the galactic gravitational potential. Based on P90 gravita-

tional potential we consider the evolution of a two-component Maxwellian initial random velocity distribution (we adopt the velocity distributions of NSs at birth from Arzoumanian et al. (2002) and Faucher-Giguère & Kaspi (2006)). We perform integration of NS velocities using Monte Carlo integration techniques with different conditions developed for this purpose. We also aim at obtaining the NS trajectories under variety of assumptions.

The paper is structured as follows: in Sec. 2 we describe the ingredients of the simulation, i.e. the NS initial position and velocity distribution and the Galactic gravitational potential. We present the results of the simulation in Sec. 3 and 4. In Sec. 3 we investigate the NSs orbits; while in Sec. 4 we investigate their vertical and radial distributions. We fit the two exponential decay model, for each spacing segment of R to derive the high scale heights. We fit also the R distributions at different scale heights. We discuss our results and their possible implications in Sec. 5.

2. Simulation ingredients

In this Section we present the ingredients of the model: the NS birth rate and Monte Carlo simulation; the gravitational potential; the position distributions of NSs; and the initial velocities and equations of motion.

2.1. NSs birth rate and Monte Carlo simulation

Theoretically, estimating the birthrate of a population of sources is simple. However, for the NS population, precise estimates of both the number and lifetime of the sources are hard to obtain, because they may have been heavily biased by a number of observational selection effects. The birthrate of NSs (η) within the whole Galactic disk is roughly $0.9 \sim 2$ per century (Lyne & Graham-Smith 2007; Lorimer 2008). If one assumes a life time $\tau \sim 10^9 - 10^{10}$ yr, then an estimate of the total number of NSs is:

$$N = \tau * \eta \simeq 10^{7-8} \quad (1)$$

The problem is best tackled using a Monte Carlo simulations of NS positions, orbits and velocities, taking into account the birthplaces and

the initial kick velocities. We study the resulting phase spatial distributions concerning the Galactic potential and the distribution of progenitors and birth velocities, focusing on the numerical properties of the NS populations in the disk and in the solar neighborhood. NS orbits are obtained by solving the equations of motion in the P90's gravitational potential.

2.2. Galactic gravitational potential

It is known that the Galactic gravitational potential causes oscillation of objects along the direction perpendicular to the Galactic plane (see e.g. Lyne et al. (1982), and references therein). To track the evolution and motion of NSs population, the gravitational potential P90 is taken to be a homogeneous function of the density, and ignore the interstellar friction. This is a reliable approximation for our axisymmetric model, because the steady state distribution of old NSs depends only weakly on the non-homogeneous part of the galactic potential (Frei et al. 1992). Asymmetry in the kinematics, which is likely due to the finite lifetime of the stars and Galactic potential structure, is a relatively small effect (Perets et al. 2009). However, using P90 may not be a good approximation when studying non-axisymmetric models, because rotating non-axisymmetric components (like bar or spirals) can introduce resonances (see e.g. Patsis & Grosbøl (1996), Patsis et al. (2002)).

Our evolution calculations are presented to simulate more realistic old NS distribution under the two-component Maxwellian initial random velocity. We model the gravitational potential of the Galaxy following P90:

$$\Phi = \Phi_{\text{sph}} + \Phi_{\text{disk}} + \Phi_{\text{halo}} , \quad (2)$$

where Φ_{sph} , Φ_{halo} and Φ_{disk} are the spheroid, halo and disk components, respectively.

For the spheroid and disk components one has:

$$\Phi_i(\mathbf{R}, z) = - \frac{GM_i}{\sqrt{R^2 + [a_i + (z^2 + b_i^2)^{1/2}]^2}} \quad (3)$$

where $R = \sqrt{x^2 + y^2}$ is the distance from the Galactic rotation axis and z is the distance from the Galactic disk plane. The subscript ‘‘i’’ represents ‘‘sph’’ and ‘‘disk’’. The values for the parameters are taken from P90 and for the spheroid component they are: $a_{\text{sph}} = 0.0$ kpc, $b_{\text{sph}} = 0.28$ kpc

and $M_{\text{sph}} = 1.12 \times 10^{10} M_{\odot}$; while for the disk component: $a_{\text{disk}} = 3.7$ kpc, $b_{\text{disk}} = 0.20$ kpc and $M_{\text{disk}} = 8.01 \times 10^{10} M_{\odot}$.

The halo component of the Galactic gravitational potential is:

$$\Phi_{\text{halo}} = \frac{GM_{\text{halo}}}{r_c} \left[\frac{1}{2} \ln \left(1 + \frac{R^2 + z^2}{r_c^2} \right) + \frac{r_c}{\sqrt{R^2 + z^2}} \arctan \left(\frac{\sqrt{R^2 + z^2}}{r_c} \right) \right] \quad (4)$$

where $r_c = 6.0$ kpc and $M_{\text{halo}} = 5.0 \times 10^{10} M_{\odot}$.

2.3. NS initial position distribution

It is generally accepted that the galactic z -distribution of massive objects is approximately exponential (Binney & Merrifield 1998; Mdzinarishvili & Melikidze 2004). This kind of the distribution can be theoretically explained by considering the dynamic equilibrium within the Galaxy. The initial z probability density function of NSs in the Galaxy has been proposed by Gott et al. (1970) and adopted by many authors since then (e.g. Gonthier et al. (2002)):

$$p_z(z) = \frac{1}{2h_z} \exp \left[\frac{-|z|}{h_z} \right] \quad (5)$$

where $h_z = 0.07$ kpc is the scale height and:

$$\int_0^{\infty} \frac{1}{h_z} \exp \left[\frac{-|z|}{h_z} \right] dz = 1 \quad (6)$$

For the initial radial probability density function of the NSs we adopt the same expression as Arzoumanian et al. (2002). As in P90, it follows a gamma function $\Gamma(2, 4.5)$, but has a radial outer boundary at 15 kpc rather than at 20 kpc¹. This is motivated by the radial distribution of NS progenitors, i.e. population I massive stars. Although the Galaxy is believed to have a stellar disk $0 \sim 15$ kpc and a gaseous disk $15 \sim 25$ kpc, NS progenitors hardly form in the gaseous disk, due to the considerable decrease of the gas density (Jones & Lambourne 2004).

¹Because of the rapid decrease of the Gamma function with R we do not expect this modification to have a large impact on the results.

The initial radial probability density function that we use is the following:

$$p_R(R) = a_r \frac{R}{R_{\text{exp}}^2} \exp[-R/R_{\text{exp}}], \quad (7)$$

where

$$a_r = \left[1 - \exp^{-\frac{R_{\text{max}}}{R_{\text{exp}}}} \left(1 + \frac{R_{\text{max}}}{R_{\text{exp}}} \right) \right]^{-1}. \quad (8)$$

We use $R_{\text{exp}} = 4.5$ kpc, which gives $a_r \simeq 1.183$. The probability distribution is normalized to 1 within the considered radial domain, i.e. from 0 to 15 kpc.

2.4. NS initial velocity distribution and equations of motion

The NS initial velocity is **calculated as** the vector addition of three different velocities: (1) a Maxwellian distribution, (2) a constant kick, and (3) the circular rotation velocities at the birth-place.

Maxwellian distributions are usually used to represent the observed distribution of pulsar velocities. In this work we choose a two-component Maxwellian distribution. One component includes 40% of all NSs and has a velocity dispersion $\sigma_v \sim 90$ km/s. The other one includes the remaining 60% and has $\sigma_v \sim 500$ km/s, as proposed by Arzoumanian et al. (2002).

While for the kick velocity we adopt the conventional value of about 400 km/s for every single object (Hansen & Phinney 1997; Hobbs et al. 2005).

The initial circular rotation velocity of the NS is determined by

$$v_{\text{circ}} = \left(R \frac{d\Phi}{dR} \right)^{1/2}, \quad (9)$$

where Φ is the P90's gravitational potential in Eq. (3).

The differential equations that describe the NS motion in the Galaxy can be expressed in the compact vector form as

$$\ddot{\mathbf{r}} = -\tilde{\nabla}\Phi \left(\sqrt{x^2 + y^2}, z \right), \quad (10)$$

where $r = \sqrt{x^2 + y^2 + z^2}$ is the spherical distance from the galactic center. NS orbits are numer-

ically integrated with the fourth-order Runge-Kutta method.

The NS total energy integral is used to control the accuracy of the integrations and in our simulations the total energy change is less than 1 part in 10^6 . The accuracy changes for different orbits, and generally simpler orbits are more accurate.

3. NS orbits in the Galaxy

The Poincaré section technique is a way of presenting a trajectory in (n) -dimensional phase space in an $(n - 1)$ -dimensional space. By picking one phase element constant and plotting the values of the other elements each time the selected element has the desired value, an intersection surface is obtained. This technique has been used by several authors (e.g. Katsanikas & Patsis (2011)) to analyze the structure of phase space in the neighborhood of stable periodic orbits in a 3D potential, and the properties of the invariant tori in the 4D spaces of section, under different galactic potentials. We use it here to study the 3-D NS trajectories and their 2-D projections.

We plot the Poincaré section for $x > 0$, and we fix $y = 0$ to investigate the dynamical 3-D orbits of NSs, as illustrated in row C in Fig. 1, with varying the initial parameters. The phase space of NS's motion is 6-D, but since the total energy and angular momentum are conserved it is in fact only 4-D and its Poincaré section is 3-D. The initial condition (x, y, z, v_x, v_y, v_z) is reported under the corresponding column in the Figure. The NSs' motions are very diversified.

Wei et al. (2010b) investigated the gravitational potential of the Galactic disk and orbits of stars, and found that all of the orbits are symmetric with respect to the galactic plane. Here we use the P90 gravitational potential and find that there are some non-symmetric orbits, see row D, columns β and γ in Fig. 1. In row A we can see that when the motion range in the vertical direction becomes larger than the one in the radial direction, the orbits become more irregular. See also same behavior for the projection on x-y plane in row B. While from row E, we see that the intersection points distribute in some regular lines on the projection of the Poincaré section, which is essentially a closed curve. As such, the

motion appears as a quasiperiodic orbit. However if the motion were exactly periodic, we would expect that after some time, the star should return back to the same intersection point on the surface section, and this is not always the case in our simulations.

According to P90, the dynamical behavior of NS populations is insensitive to the initial scale-height of progenitors. Here we see that NS orbits are like those of their progenitors: they are all basically rotating around the Galactic center, at different radial distance and uniformly.

4. Simulation Results and Discussions

In our calculation we obtain that the NS distribution is steady after 10^9 yr. After this time we see that the NSs have greatly expanded in the radial direction, with the majority of them being located beyond 25 kpc from the Galactic center. More precisely 80% of the old NSs remains within 25 kpc from the Galactic rotation axis (i.e. $R < 25$ kpc), and 18% instead remains within 25 kpc from the Galactic center (i.e. $r < 25$ kpc). NSs moving in and out of the above range are in a dynamically equilibrium state.

4.1. Radial distribution of NSs

As we mentioned earlier, NSs are born in the region 0 – 15 kpc and later on they spread to all radii. We follow an approach similar to Wei et al. (2010b) in order to investigate the characteristics of old NS distribution under the two-component Maxwellian initial random velocity. The normalized position probability density function that we find is shown in Fig. 2. We find that the distribution deviates from the initial distribution, i.e. $\Gamma(2, 4.5)$, due to the NS motion in the Galactic gravitational field. The distribution peak is now closer to the Galactic center. At first we fit the normalized R probability density function with the Gamma function $\Gamma(\alpha, \lambda)$ as:

$$p_R(R) = A \frac{R^{\alpha-1}}{\lambda^\alpha} \exp^{-R/\lambda} . \quad (11)$$

The best fitting Gamma function is $\Gamma(1.7, 5.2)$. The peak location of a generic Gamma function $\Gamma(\alpha, \lambda)$ is at $r_p = \lambda(\alpha - 1)$. Using this expression for the initial radial distribution we get 4.5 kpc, while for the simulated distribution the peak is at

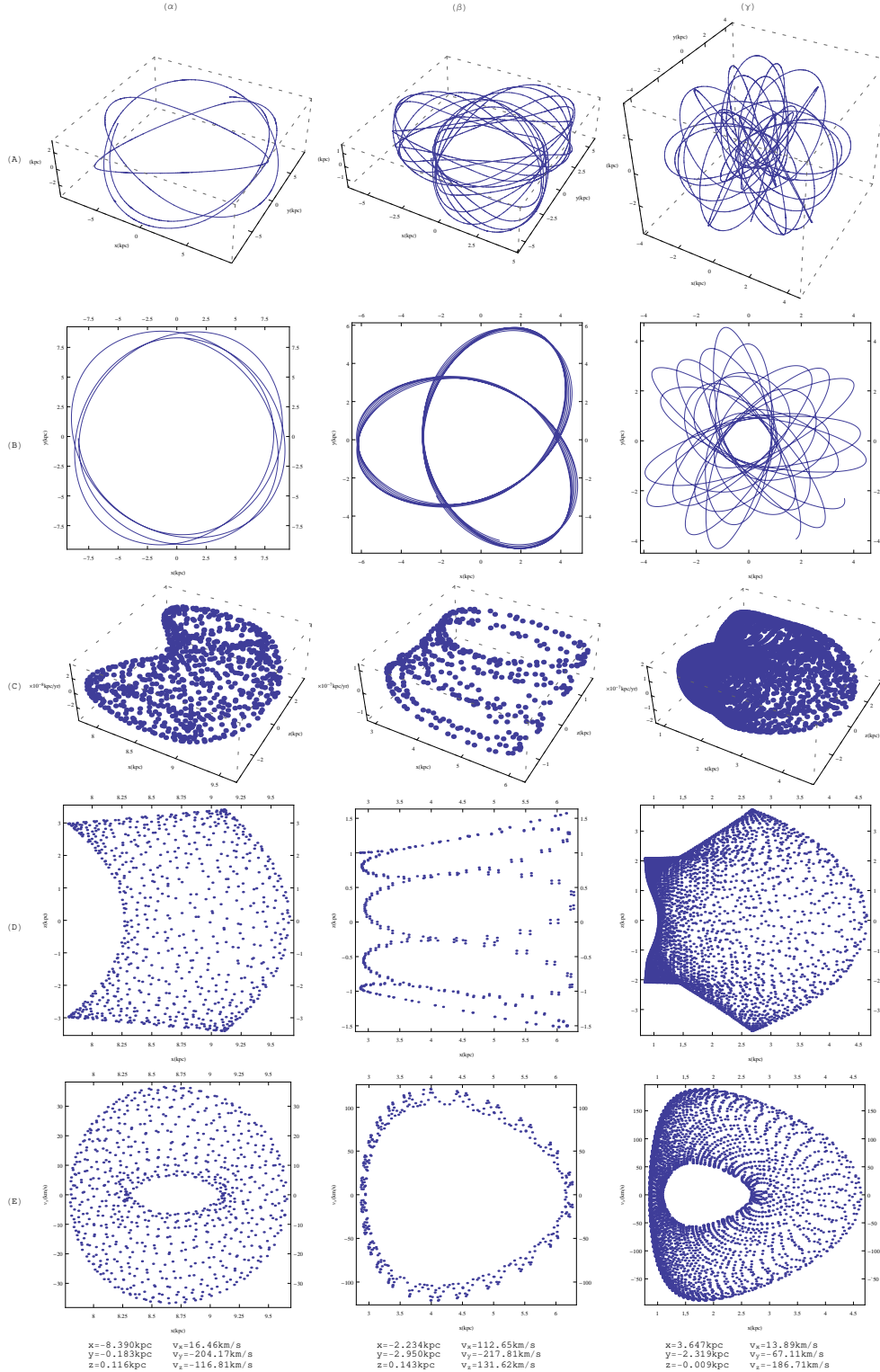


Fig. 1.— 3-D orbits of NSs. Panels in row A: trajectories; panels in row B: projections of the trajectories on the galactic plane; panels in row C: Poincaré section $x > 0, y = 0$ of the 3-D trajectory; panels in row D: projections on $x-z$ plane of the Poincaré sections; panels in row E: projections of the Poincaré sections on $x-v_x$ plane.

3.71 ± 0.17 kpc. The fitting results are listed in Tables 1, 2 and 3.

Due to the unsatisfactory fitting of Gamma function, specially at the peak, we use the “zero point corrected $\Gamma(\alpha, \lambda)$ ” proposed by Wei et al. (2010b). **They** modify the Gamma function $\Gamma(\alpha, \lambda)$ by adding a constant A_0 :

$$p_R(R) = A_0 + A \frac{R^{\alpha-1}}{\lambda^\alpha} \exp^{-R/\lambda}, \quad (12)$$

If the points are close to a Gamma distribution function then the scatter will be small relative to the total variation in the values of the response variable. We adopt the coefficient of determination (COD, also known as r-squared) to measure the fit quality. The closer COD to 1, the better the fit. Figure 2 indicates that the Gamma distribution function is quite satisfactory with a COD of 0.99, and Eq. (12) is acceptable for the case with the relative standard errors of the fitting parameters less than 5%.

As for the Γ function, also for the “zero point corrected Γ ” the peak position is at $\lambda(\alpha - 1)$ and for the best fit case it is at 3.73 ± 0.19 kpc. We notice that the evolution of the NSs in the Galactic gravitational field makes the value of their R -distribution at $R = 0$ kpc not exactly equal to 0. In other words, there is a “zero shift”, which is the total effect of the NS orbits shown in Sec. 3

4.2. Vertical distribution of NSs

We consider the vertical distribution of the bound NSs in the whole Galactic disk with $R < 25$ kpc and we find that it is not well described by a single exponential decay. For this reason we employ a double exponential profile:

$$p_z(z) = A_0 \times g(z) + A_1 \times \exp[-z/h_1] + A_2 \times \exp[-z/h_2], \quad (13)$$

where $A_0 \times g(z)$ represents the disk component, $g(z)$ is step function which is 1 in the disk and 0 outside, and h_1 and h_2 are the height scales of the two exponential contributions. Without loss of generality we can assume $h_1 < h_2$ and refer to $A_1 \times \exp[-z/h_1]$ as the low-scale-height component and to $A_2 \times \exp[-z/h_2]$ as the high-scale-height component. The probabilities for the low-scale-height and the high-scale-height component

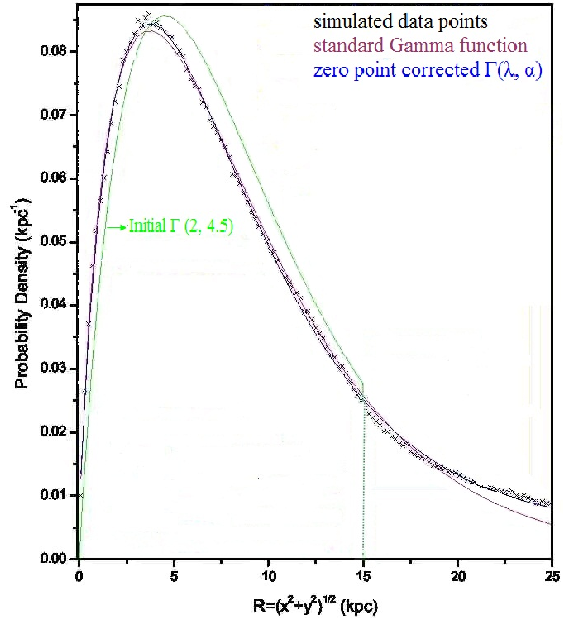


Fig. 2.— Radial probability density distribution. The crosses (black) indicate simulated data points; the dotted (green) line indicates the initial Gamma function; the two solid lines indicate the best fit with the “zero point corrected $\Gamma(\alpha, \lambda)$ ” (blue), and with the standard Gamma function (brown). Details about the fits are given in Tables 1, 2 and 3, respectively.

are respectively:

$$P_1 = \int_0^\infty A_1 \times \exp[-z/h_1] dz = A_1 \times h_1 \quad (14)$$

$$P_2 = \int_0^\infty A_2 \times \exp[-z/h_2] dz = A_2 \times h_2. \quad (15)$$

We also study the half density scale height of the disk $z_{1/2}$, defined as the height at which the **total** probability density drops to 50% of the Galactic plane one. These results are shown in Table 1. We get a COD ~ 0.99 and relative standard errors $\lesssim 1\%$, except that the relative standard error of p_0 lies in the range 6.4 %.

Table 1: Parameters of two exponential decay model Eq. (13).

parameter	value	relative error %
$A_0(\text{kpc}^{-1})$	1.8×10^{-5}	6.4
$A_1(\text{kpc}^{-1})$	1.87	0.02
$h_1(\text{kpc})$	20.6×10^{-3}	0.04
$A_2(\text{kpc}^{-1})$	35.6×10^{-3}	0.09
$h_2(\text{kpc})$	1.55	0.08
COD	0.999	-
P_2/P_1	1.45	0.003
$z_{1/2}(\text{kpc})$	17.6×10^{-3}	0.01

Table 2: Best fit results for the standard Gamma function.

parameter	value	relative error %
A	1.13	0.49
α	1.71	0.54
$\lambda(\text{kpc})$	5.21	0.86
COD	0.996	-

Observational studies of the Galactic disk reveal that it can be well described in terms of the two components model with a thin disk and a thick disk component (see e.g. Chen et al. (2001), Kaempf et al. (2005), Wei et al. (2010a)). Our simulation confirms the validity of this model

Table 3: Best fit parameters for the “zero point corrected $\Gamma(\alpha, \lambda)$ ”.

parameter	value	error %
$A_0(\text{kpc}^{-1})$	5×10^{-3}	6.3
A	95.6×10^{-3}	1.2
α	1.83	0.58
$\lambda(\text{kpc})$	4.48	1.1
COD	0.998	-

Table 4: Best fit parameters for linear relations of the radial distributions of the two scale heights h_1 and h_2 .[†] is for fitting the region inward of 4.25 kpc and [‡] is for fitting the region outward.

parameter	value	error %
k_1	13×10^{-3}	0.26
b_1	12.8×10^{-3}	0.005
k_2^\dagger	18.4×10^{-3}	0.0007
b_2^\dagger	0.03	0.002
k_2^\ddagger	0.05	0.66
b_2^\ddagger	0.65	0.16

and shows that the z hierarchy effect can be regarded as the result of the dynamical evolution of the old NSs originated from the Galactic disk.

4.3. Scale-Height vs R relation

We now consider the z distribution at different Galactic radial distances R from the Galactic center. To this end, we divide R with 0.5 kpc spacing from 0 kpc to 25 kpc and get 50 parts, then we analyze in details the NS z distribution in each part. The two exponential decay of Eq. (13) is still employed to study the case in each spacing segment of R , to derive the high-scale-heights h_2 , low-scale-heights h_1 , and the ratios of the two components P_2/P_1 .

The results are shown in Fig. 3. In each segment of R the two exponential model is still significantly effective. As a result, the CODs of both distributions in Fig. 3 is quite similar ~ 0.99 , and

with very small relative standard errors $\lesssim 0.01$. The fitting results are listed in Table 4.

The relationship between the two scale heights and R can be described by the following linear model.

$$h(R) = k \times R + b, \quad (16)$$

We also plot the radial dependence of the half density scale heights in Fig. 3. The fitting results of parameters k and b are listed in Table 4.

The low-scale-heights can be depicted by a linear function of R within the whole range of the Galactic disk $0 - 25$ kpc. The slope of the fitting line is small, which means that the changing of this component within $0 - 25$ kpc of R is not large.

For the high-scale-height components, there exists a point at $R = 4.25$ kpc, where the behavior changes. Both sides of this point have a linear radial dependence but with different slopes: the one inside $R < 4.25$ kpc is smaller than the one outside $R > 4.25$ kpc. We notice that $R = 4.25$ kpc corresponds to the observed R_0 of the HI disk.

As regards the R distribution of P_2/P_1 , we can see the difference of old NS distribution under Arzoumanian et al. (2002) from those under Hobbs et al. (2005) and Faucher-Giguère & Kaspi (2006) in Wei et al. (2010b). Where the R distributions of P_2/P_1 have three distinct parts clearly, and the high-scale-height distributions have not points like the observed R_0 of the HI disk. The ratio of the two components leads to the increase of growth slowly and smoothly with R in the whole Galaxy.

Table 5: Best fit parameters for linear relations of the radial distributions of the half density of two scale heights Eq. (16).

parameter	value	error %
k	14.9×10^{-3}	0.01
b	10.5×10^{-3}	0.01

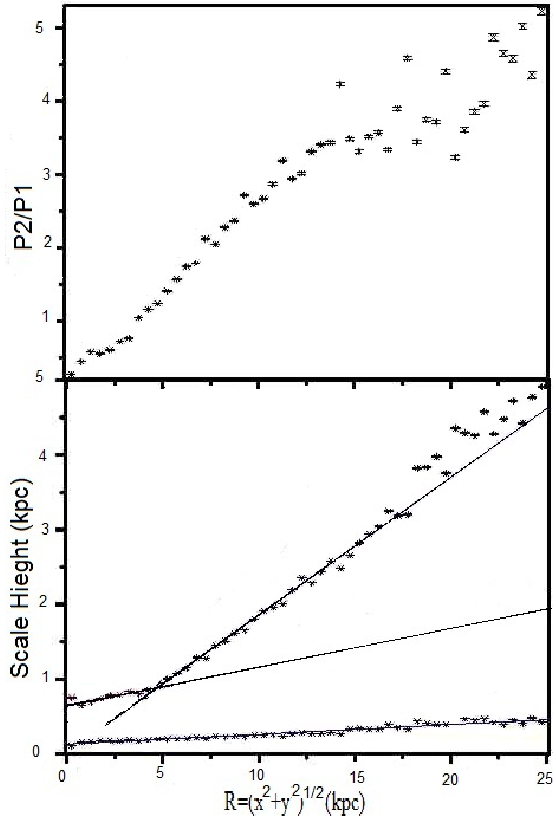


Fig. 3.— Scale-heights in the double exponential decay model see Eq. (13). Top panel: ratio of P_2/P_1 . Bottom panel: radial distributions of the two scale heights h_1 and h_2 . For both of the panels the crosses indicate simulated data points, while the solid lines indicate the best fit line. The fitting parameters are given in Table 4.

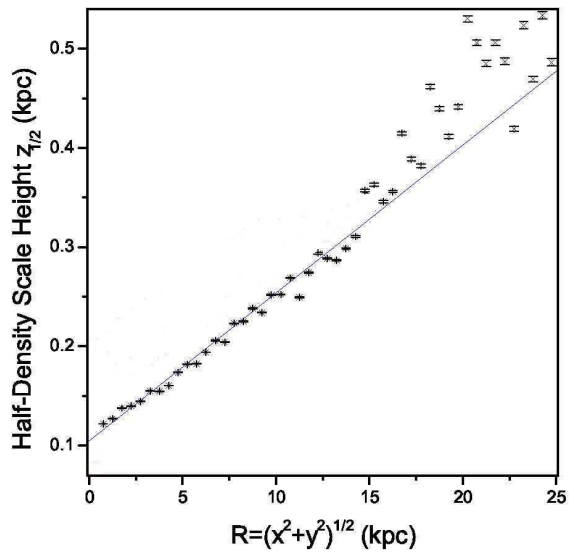


Fig. 4.— Radial distributions of the half density scale heights in the region $R < 25$ kpc with the fitting parameters of Eq. (16) for the straight lines.

The NS scale-heights generally increase from the Galactic center to the edge of Galactic disk. This phenomenon is independent of the initial velocity distribution of the NSs, and it is due to the action of the Galactic gravitational field on the NSs. Our calculation shows that the heights of the orbits of the NSs generally decrease towards the Galactic center (see Sec. 3). P90 calculated the half density scale height in the vicinity of the Sun ($R_0 = 8$ kpc) and obtained $z_{1/2} = 0.2$ kpc. In our present updated version the corresponding value is 0.2 ± 0.0004 kpc.

5. Discussions and Conclusions

In this paper we have investigated the space and velocity distribution of old neutron stars (NSs) in our Galaxy. We assume that the initial velocity distribution is the result of three components: the kick velocity, the circular velocity and the Maxwellian velocity (following Arzoumanian et al. (2002)). For the initial position distribution instead we assume that it follows a Γ function. As regards the Galactic gravitational potential, we follow the Paczyński (1990) prescription, which is of course only an approximation, since it does not take into account any inhomogeneity within the Galaxy. However this is suitable for the simplified analysis that we are developing here. We have then used Monte Carlo simulations to let the NSs evolve and have shown 3-D NS orbits and Poincaré sections of the phase space.

It is evident that the irregular character of the motion of NSs increases when the vertical direction becomes larger than radial direction. Another remarkable finding is that there are some significant diffractions in the symmetric of the orbits, which may have effects of supernovae kicks.

Our numerical results show that NSs have a very large radial Galactic expansion. The majority of them (80%) falls within 25 kpc from the Galactic rotation axis ($R < 25$ kpc), and 18% instead remains within 25 kpc from the Galactic center ($r < 25$ kpc). An important aspect is that the total number of NSs moving in and out of the above range is in a dynamically equilibrium state after 10^9 yr.

The radial probability density distribution deviates from the initial distribution, and has a peak

which is closer to the Galactic center. The analysis of the vertical and radial distributions clearly show that the orbits of the NSs decrease toward the Galactic center within different scale heights.

Qualitatively, the simulated old NSs disk, especially the middle and outer components, keeps the observed HI disk in moderation. Although the old NSs and their progenitors have different radial and vertical distribution, we find that the shapes of their orbits are quite similar in the HI clouds regions.

The results of this work will constitute the base for further studies on NS properties. Such research could be helpful for the detection of old NSs via their gravitational microlensing that result in the variation in the brightness of the distant active galactic nuclei (e.g. Hawkins (1993, 2002)). Another way for detecting the old NSs is through the interaction with the interstellar medium (Popov et al. 2000).

As subsequent steps we plan to (1) apply the three exponential decay model in studying the NS vertical distribution with more detail and (2) to use different models of the Galactic potential to investigate specific parts of our Galaxy.

Acknowledgments

This work is supported by the National Natural Science Foundation of China (NSFC 10773017, NSFC 10773034) and National Basic Research Program of China (2009CB824800, 2012CB821800). Chinese Academy of Sciences and National Astronomical Observatory of China (NAOC) of CAS has supported this work by the Silk Road Project (CAS Grant Number 2009S1-5). L.N. is currently supported by a Chinese Academy of Sciences fellowship for young international scientists (Grant Number 2010Y2JB12).

REFERENCES

- Arzoumanian, Z., Chernoff, D. F., & Cordes, J. M. *Astrophys. J.* **568**, 289 (2002)
- Bhattacharya D. & van den Heuvel E. P. J., *Phys. Rep.*, **203**, 1 (1991)
- Binney J. & Merrifield M., *Galactic Astronomy* (Princeton: Princeton University Press) (1998)

- Caldwell J. & Ostriker J., *Astrophys. J.* **251**, 61 (1981)
- Chen B., Stoughton C., Smith J. A., et al. *Astrophys. J.* **553**, 184 (2001)
- Cordes J. M., & Chernoff D. F., *Astrophys. J.* **505**, 315 (1998)
- Cordes, J. M., & Lazio, T. J. W. arXiv:astro-ph/0207156 (2002)
- Faucher-Giguère C.-A. & Kaspi V. M., *Astrophys. J.* **643**, 332 (2006)
- Frei Z., Huang X. & Paczyński B., *ApJ.* **643**, 332 (1992)
- Gonthier P. L., Ouellette M. S., Berrier J. et al. *Astrophys. J.* **565**, 482 (2002)
- Gott J. R., Gunn J. E., & Ostriker J. P., *Astrophys. J.* **160**, L91 (1970)
- Hansen B. M. S. & Phinney E. S., *Mon. Not. R. Astron. Soc.* **291**, 569 (1997)
- Hawkins M.R.S., *Nature* **366**, 242 (1993)
- Hawkins M.R.S., *Mon. Not. R. Astron. Soc.* **329**, 76 (2002)
- Hobbs G., Lorimer D. R., Lyne A. G., & Kramer M., *Mon. Not. R. Astron. Soc.* **360**, 974 (2005)
- Jones M. H, & Lambourne R.J.A. *An Introduction to Galaxies and Cosmology*. Cambridge: Cambridge University Press, 7 (2004)
- Kaempf T. A., de Boer K. S., & Altmann M., *Astron. & Astrophys.* **432**, 879 (2005)
- Katsanikas M. & Patsis P. A., *Int. J.Bif. Chaos*, **21**, 467 (2011)
- Lorimer D. R. *Living Rev. Relativity*, **11**, 8 (2008)
<http://relativity.livingreviews.org/Articles/lrr-2008-8/>
- Lyne A. G., Anderson B., & Salter M. J., *Mon. Not. R. Astron. Soc.* **201**, 503 (1982)
- Lyne A. G., Burgay M., Kramer M. et al. *Science*, **303**, 1153 (2004)
- Lyne A. G. & Graham-Smith, F., *Pulsar Astronomy*, Cambridge Astrophysics Series, Cambridge University Press, 3ed Edit. (2007)
- Mdzinarishvili T. G. & Melikidze G. I., *Astron.& Astrophys.*, **425**, 1009 (2004)
- Ofek E. O., *PASP*, **121**, 814 (2009)
- Paczynski B., *Astrophys. J.* **348**, 485 (1990)
- Patsis P. A. & Grosbøl P., *Astron.& Astrophys.*, **315**, 371 (1996)
- Patsis P. A., Athanassoula E., Grosbøl P. et al. *Mon. Not. R. Astron. Soc.* **355**, 1049 (2002)
- Perets H. B, Wu X., Zhao H. S. et al. *ApJ*, **697**, 2097 (2009)
- Popov S. B., Colpi M., Treves A. et al. *ApJ*, **530**, 896 (2000)
- Sartore N., Ripamonti E., Treves A. & Turolla R., *Astron.& Astrophys.*, **510**, A23 (2010)
- Taylor J. H., & Cordes J. M., *Astrophys. J.* **411**, 674 (1993)
- Wei Y. C., Taani A., Pan Y. Y. et al., *Chin. Phys. Lett.*, **27**, 9801 (2010a)
- Wei Y. C., Chengmin C. M., Xinji W. et al., *Science in China*, 53, 1939 (2010b)